3-D-Hierarchical Signalling for Resilient Optical Wireless Communication Systems

EGECAN GULER[1], CALLUM T. GELDARD[1], IAIN BUTLER[2], TRIO ADIONO[3] (Senior Member, IEEE), AND WASIU O. POPOOLA[1] (Senior Member, IEEE)

[1]Institute for Imaging, Data and Communications, School of Engineering, The University of Edinburgh, Edinburgh EH9 3BF, U.K.

[2]UK Defence Science and Technology Laboratory, SP4 0JQ Salisbury, U.K.

[3]School of Electrical Engineering and Informatics, Institut Teknologi Bandung, Bandung 40132, Indonesia

CORRESPONDING AUTHOR: E. GULER (e-mail: s1553558@sms.ed.ac.uk)

ABSTRACT This paper presents a 3 dimensional (3D)-hierarchical modulation technique for optical wireless communication (OWC) systems in which high, medium and low priority data are encoded on the frequency, phase and amplitude of a subcarrier signal, respectively. The error performance of the 3D-hierarchical modulation is derived and evaluated under different channel conditions. A proof-of-concept experiment is then presented to demonstrate the feasibility of this approach. The results presented in this study show that encoding high and medium priority data on the frequency and phase of a subcarrier signal offers resilience against the deleterious effects of the OWC channel. The amplitude dimension of the subcarrier signal can then be utilised to further increase the system spectral efficiency if the channel conditions allow for it.

INDEX TERMS Optical wireless communications (OWC), underwater optical wireless communications (UOWC), visible light communication (VLC), free-space optical communication, modulation schemes, signalling techniques for OWC.

I. INTRODUCTION

OPTICAL wireless communication (OWC) as a technology that encompasses VLC, LiFi, FSO etc, is an emerging field that is gaining increased attention [1], [2]. OWC technology is suitable in environments where radio frequency (RF) transmission is inhibited, undesirable or impractical such as in underwater and RF sensitive areas. For example, underwater optical wireless communication (UOWC) systems can support high data rate, low-latency connectivity over short link distances (10s of metres) when compared to the dominant underwater acoustic communications (UAC) [3]. Thus, to sustain ubiquitous wireless connectivity that is the backbone of our socio-economic activities, OWC has a vital role as a complementary technology to the existing UAC and RF-based communication systems.

Recent progress in OWC include the works described in references [4], [5], [6], [7], [8], [9], [10], [11], [12], [13], [14], [15], [16], [17], [18], [19], [20], [21], [22], [23], [24], [25], [26], [27], [28], [29], [30], [31], [32]. In [6], a cellular network integrated free-space optics (FSO) system was proposed that considers channel effects due to weather conditions. In [7], a fully networked indoor visible light communication (VLC) system was investigated. Other studies have focused on increasing the maximum achievable transmission rate of OWC by making an efficient use of the available modulation bandwidth. Including in [8], where transmission rates of 56 Gbps per optical source was demonstrated in a fibre-FSO system over 500 m in free-space utilising pulse amplitude modulation (PAM). Similarly, a 30 Gbps UOWC system was realised with 4-PAM in [9]. These works showcase the benefit of OWC in terms of the maximum data rates achieved in experimental works. Modulation techniques that utilise subcarrier intensity modulation (SIM), including orthogonal frequency division multiplexing (OFDM) and discrete multi-tone (DMT) modulation, have been researched extensively in order to exploit the whole modulation bandwidth [13], [14], [15],

[16], [17], [18], [19], [20], [21], [22], [23], [24], [25]. In [11], [15], phase-shift keying (PSK) was investigated as a suitable technique for OWC systems and its error performance in fading channels are presented showing the benefits of encoding data on the phase of the carrier signal. Frequency-shift keying (FSK) was investigated as an energy efficient modulation scheme that can operate in fading channels in [12]. The FSK technique was implemented using OFDM in [16] for RF-based communication systems. FSK was additionally analysed and presented as a suitable modulation scheme for VLC systems to achieve high energy efficiency in [17]. In our previous work in [18], we demonstrated the resilience of FSK implemented using SIM in a turbulent UOWC channel. In [21], a VLC system using quadrature amplitude modulation (QAM) with OFDM scheme was improved with the use of probabilistic shaping and wavelength division multiplexing (WDM) to demonstrate a transmission rate of 10.8 Gbps. In [22], a QAM-DMT technique was used to achieve 20 Gbps in an underwater scenario. In [22], [23] optical front-ends and transmission techniques exploiting the wavelength and polarisation of the optical signal to optimise the transmission rate for UOWC systems were investigated. Other works in UOWC have demonstrated operational systems carrying out high quality video transmission and underwater autonomous vehicles data muling in sensor networks underseas [26], [28]. With practical applications in mind, self-powering devices utilising simultaneous light and power transfer (SLIPT) technology have been envisioned [29], [30], [31], [32]. This recent research demonstrates the feasibility of OWC in many different practical applications scenarios from underwater, to terrestrial and indoor. However, there is still the challenge of OWC waveform design that is resilient to the different hostile channel effects in these different application areas.

This study presents a 3D-hierarchical signalling that utilises subcarrier intensity modulation to implement a signalling technique that provides resilience against a number of channel effects common in OWC applications. In this approach, a sinusoidal subcarrier signal, $x(t)$, is used to modulate the intensity of an optical source. Thus, $x(t)$ becomes the envelope of the emitted light intensity that can be recovered via direct detection at the receiver. The three-dimensions of frequency, phase and amplitude of $x(t)$ are now available to encode the data. This is done hierarchically for resilience, with the high priority data encoded on the frequency of $x(t)$, followed by phase and the least priority data on the amplitude. Thus, the first and second order priority data are resilient to channel impairments (such as turbulence) that significantly affect the received optical intensity.

Consequently, SIM permits the implementation of frequency-shift keying; phase-shift keying and quadrature amplitude modulation on the intensity of a light source. Through this technique, a simultaneous phase and frequency-shift keying (PFSK) scheme, like the one introduced in [33] and adapted to optical communications in [34], can also be implemented. We develop this idea further by deriving the analytical performance of PFSK and simultaneously use the amplitude as the third dimension to encode the data. The resulting 3D-hierarchical modulation, phase, amplitude and frequency-shift keying implemented using SIM, is abbreviated to PAFsk-SIM where modulation orders M_f, M_p and M_a refer to the frequency, phase and amplitude components of the subcarrier signal, $x(t)$ respectively. In this paper, the spectral and energy efficiency of the PAFsk-SIM scheme is discussed and its performance in three different channel conditions investigated.

The paper is structured as follows: Section II introduces the channel effects considered in this study; Section III describes OWC system, generation and decoding of PAFsk-SIM; Section IV presents bit error rate performance of the PAFsk-SIM in additive white Gaussian noise (AWGN) and fading channels; Section V contains performance results in three different channel conditions while Section VI presents an experimental case study in an underwater channel; concluding remarks are given in Section VII.

II. OWC CHANNEL EFFECTS
In this section the channel effects considered in this work are briefly introduced. These are:

- Turbulence induced fading, modeled using log-normal distribution.
- Multipath propagation caused, by either reflections in an indoor scenario or due to multiple scattering in an underwater channel.

The first channel effect considered in this paper is turbulence induced fading. This presents a key challenge for FSO and UOWC links. Turbulence affects the coherent light sources on a greater scale, thus it is most relevant for systems employing a laser diode [35]. Turbulence can be understood as a random scattering event caused by refractive index changes across the path of the beam due to salinity or temperature inhomogeneity in the medium or also water bubbles in an UOWC scenario. Resultantly, the received optical power fluctuates. This can cause a burst of detection errors and reduction in the average received SNR [3], [36].

Turbulence induced fading is quantified in relation to the variance it causes in the received optical power which is called scintillation index (σ_I^2) defined as [37]:

$$\sigma_I^2 = \frac{\langle I^2 \rangle - \langle I \rangle^2}{\langle I \rangle^2}, \tag{1}$$

where I is the received optical intensity, and $\langle . \rangle$ denotes the ensemble average.

Next, the multipath effect is a challenge faced in many applications of OWC including indoor, communication between unmanned aerial vehicles (UAV) and ground station and UOWC [38], [39], [40]. Multipath propagation can be caused by light arriving at different times due to reflection off surfaces as well as particles in a medium. Effects of multipath manifest as a signal spread, causing inter-symbol interference
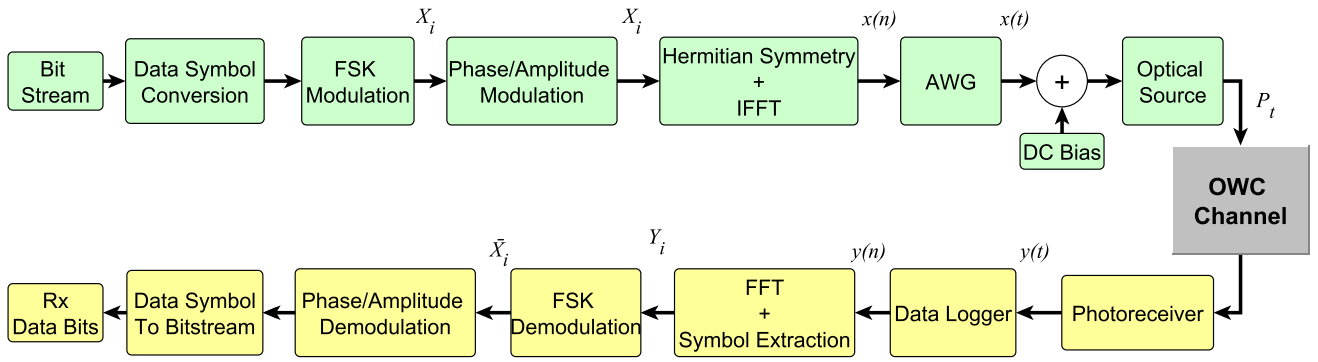
FIGURE 1. PAFsk-SIM block diagram.

(ISI). A common source of multipath propagation is from the particles suspended within the channel itself, where photons are scattered upon interaction with a particle [41]. This scattering process is most prevalent in UOWC and long range FSO links. Transmission through a highly scattering channel is subject to attenuation and beam spread [42]. Here, multiple scattering causes a multipath effect, which in turn leads to temporal dispersion at the receiver, resulting in ISI and a reduction in received signal-to-noise ratio (SNR) [43].

III. SYSTEM DESCRIPTION
This section describes the OWC system utilising SIM and details the 3D-hierarchical signal generation/decoding process.

A. SUBCARRIER INTENSITY MODULATION
In an OWC system employing intensity modulation with direct detection (IM/DD), the emitted optical power can be modeled as:

$$P_{t}(t) = P_{ave}(1 + \beta x(t)), \qquad (2)$$

where P_{ave} represents the average transmitted optical power and β is the optical modulation index. Here, data is encoded on the properties of an electrical subcarrier signal $x(t)$. In state-of-the-art, $x(t)$ is a pulse signal with data encoded on its amplitude as in on-off keying (OOK) and PAM [8], [9]. These amplitude modulation techniques are simple to implement but their performance is susceptible to the effects of the channel. Hostile channel conditions in practical situations such as multipath due to reflections, multiple scattering, and turbulence cause significant error performance degradation. For example, the ISI due to temporal dispersion in multipath channels causes the signal power to leak into neighbouring symbols. This in turn causes symbols to be decoded incorrectly in OOK. Similarly, turbulence induced fading causes fluctuations in the received optical power that affect amplitude modulated signals significantly. These fluctuations in the received power make the fixed symbol decision threshold ineffective, causing erroneous detection of OOK symbols.

With SIM, $x(t)$ is a time-continuous signal given as:

$$x(t) = \sum_{i=1}^{N_{sc}} A_i \cos(\omega_i t + \phi_i), \qquad (3)$$

where N_{sc} is the total number of subcarriers. In (3), the data can be encoded on the amplitude, A_i; the phase, ϕ_i; or the frequency component, ω_i of the subcarrier signal, $x(t)$. Utilising these properties of the carrier allows the information to be modulated over three dimensions, thus providing the opportunity to select which characteristics of $x(t)$ to encode data on based on the channel conditions.

The first of the properties considered is the frequency of the subcarrier. This is implemented as orthogonal non-coherent frequency-shift keying (FSK) which is an energy efficient technique. In addition, it offers resilience against fluctuations in amplitude or phase due to the channel and therefore used for the high priority data. In [18], [44], we have shown the resilience of SIM with FSK against underwater turbulence. In addition to this resilience, the FSK-SIM implementation is simple but it suffers from low spectral efficiency. By adding a layer of phase modulation on top of FSK, the spectral efficiency is improved while maintaining a degree of resilience to turbulence induced fading as the phase of $x(t)$ is unaffected by amplitude fluctuations caused by fading. Resultantly, the phase can be used to encode medium priority data. The amplitude and the phase of $x(t)$ can be used simultaneously to increase modulation dimension as in quadrature amplitude modulation (QAM). This comes at the expense of performance degradation due to channel effects on A_i. To further improve the spectral efficiency, the lowest priority data can be coded on the amplitude to achieve a fully 3D PAFsk-SIM with overall modulation order $M = M_f M_p M_a = M_f M_{pa}$ where M_{pa} is the QAM modulation order.

B. SIGNAL GENERATION AND DECODING
The block diagram of an OWC system using the PAFsk-SIM scheme is given in Fig. 1. The incoming serial bitstream is converted to data symbols in accordance with modulation level parameters M_f, M_p, and M_a. First, M_f-FSK-SIM is implemented, this determines the active subcarrier.
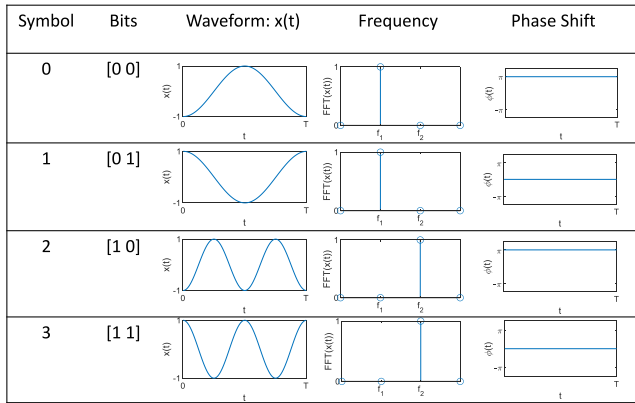
FIGURE 2. An illustration of PAFsk-SIM bit mapping for the case of $M_f = 2, M_p = 2, M_a = 1$.

FIGURE 3. The symbol error performance of PAFsk-SIM.

Subsequently, data is encoded on the phase and/or amplitude of the active subcarrier. When the subcarrier frequencies, $\omega_i, i = 0 \ldots N_{sc}$, in (3), are orthogonal, then the efficient inverse Fast Fourier transform algorithm, IFFT, can be used to digitally implement SIM as shown. The information encoded on the amplitude and phase of the i_{th} subcarrier frequency can be represented as $X_i = (A_i e^{j\phi_i})$. Thus, (3) may be written in the discrete form as:

$$x(n) = \text{IFFT}\{X\}; \qquad (4)$$

where,

$$X = \left[0, \ X_i, \ 0, \ X_i^H\right]. \qquad (5)$$

Here, X_i^H is the Hermitian component of X_i needed to ensure that $x(n)$ is real with no imaginary part. Figure 2 gives an illustration of PAFsk-SIM waveform, with $M_f = 2, M_p = 2, M_a = 1$.

The output of the IFFT operation is combined with an optimal DC-bias to drive the optical source which is intensity modulated by the information carrying electrical signal.

Following direct detection at the receiver, the incoming time domain signal is converted to the frequency-domain by the use of FFT. Detection of the subcarrier frequencies using FFT renders the decoding process non-coherent.At the receiver, index of the active subcarrier is first recovered (using FFT) followed by its phase and/or amplitude to complete the 3D demodulation. It should be noted that the scheme can be implemented to have one (i.e., FSK-SIM) or two (i.e., FSK+PSK-SIM) or all three dimensions (PAFsk-SIM). If all the subcarriers (and not their index) are used simultaneously to carry data, then this scheme will default to the OFDM technique. Thus, the non-hierarchical optical OFDM is a subset of PAFsk-SIM.

IV. ERROR PERFORMANCE ANALYSIS

This section provides the analytical error performance of PAFsk-SIM. With the frequency being the base on which the phase and amplitude hierarchies are laid; a PAFsk-SIM symbol er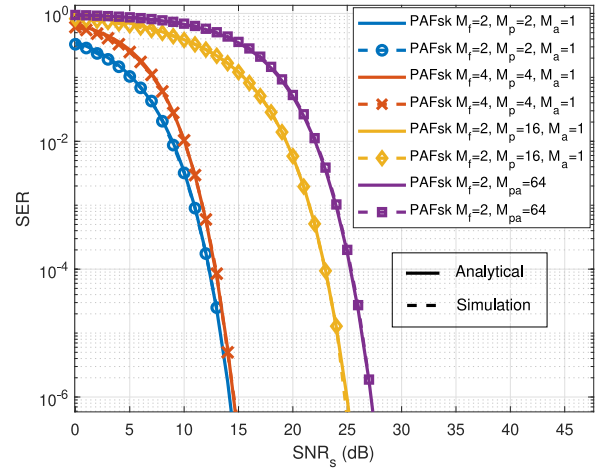ror occurs if the frequency component is decoded incorrectly or if the phase and/or amplitude components are in error following a correct frequency detection. Thus, PAFsk-SIM symbol error, $P_{e_{\text{PAFsk}}}$ becomes:

$$P_{e_{\text{PAFsk}}} = P_{e_f} + P_{e_{\text{pa}}} - P_{e_f}P_{e_{\text{pa}}}, \qquad (6)$$

where P_{e_f} and $P_{e_{\text{pa}}}$ are symbol error probabilities for the frequency and phase/amplitude components respectively. For convenience, the phase and amplitude data are encoded jointly using quadrature amplitude modulation (QAM).

The P_{e_f} expression is equivalent to the probability of error of a non-coherently decoded orthogonal FSK-SIM given as [45]:

$$
\begin{aligned}
P_{e_f} = \sum_{n=1}^{M_f-1} & (-1)^{n+1} C_n^{M_f-1} \frac{1}{n+1} \\
& \times \exp\left(-\frac{n\text{SNR}_s}{(n+1)}\right),
\end{aligned}
\qquad (7)
$$

where SNR_s is the signal-to-noise ratio per symbol. In (6), $P_{e_{\text{pa}}}$ is equivalent to the QAM symbol error expression given as [45]:

$$P_{e_{\text{pa}}} = P_{e_{\text{QAM}}} = 1 - \left(1 - P_{e_{\sqrt{M_{pa}}}}\right)^2, \qquad (8)$$

and,

$$P_{e_{\sqrt{M_{pa}}}} = 2\left(1 - \frac{1}{\sqrt{M_{pa}}}\right)Q\left(\sqrt{\frac{3}{M_{pa}-1}\text{SNR}_s}\right), \qquad (9)$$

where $Q(\cdot)$ is the Gaussian Q-function and (9) is only valid for a square constellation. If the amplitude hierarchy is not in use, then $P_{e_{\text{pa}}}$ defaults to the PSK-SIM symbol error probability, P_{e_p} given as [45]:

$$P_{e_p} = P_{e_{\text{PSK}}} = 2Q\left(\sqrt{2\text{SNR}_s}\sin\frac{\pi}{M_p}\right). \qquad (10)$$

Figure 3 shows the symbol error performances for PAFsk-SIM at different modulation orders obtained from (6) and validated with Monte-Carlo (MC) simulations. This figure
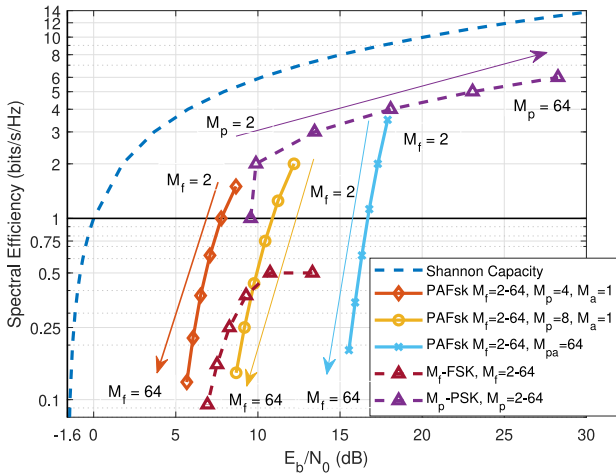
FIGURE 4. Spectral efficiency of PAFsk-SIM versus the signal-to-noise ratio needed to attain an indicative symbol error rate, $P_{e_{PAFsk}} = 10^{-5}$.

FIGURE 5. Analytical SER performances of PAFsk-SIM and OOK in log-normal turbulence with $\sigma_I^2 = 0.1$ obtained from (19).

illustrates that when the M_f and M_p are increased from 2 to 4, the required symbol power increases by less than 0.1 dB. Thus, highlighting the power efficiency of the PAFsk-SIM. To achieve higher transmission rates in a benign channel condition, modulation level M_p and M_{pa} can be increased.

The spectral efficiency, η_{PAFsk}, of PAFsk-SIM scheme is obtained by considering all the constituent modulation dimensions. In this hierarchical format, the base FSK-SIM signalling dictates the overall signal bandwidth while the total number of bits is the sum of bits encoded on each of the three dimensions. As such, an expression for the PAFsk-SIM spectral efficiency is:

$$\eta_{PAFsk} = \frac{(k_f + k_p + k_a)}{M_f}, \tag{11}$$

where $k_f = \log_2(M_f)$, $k_p = \log_2(M_p)$, and $k_a = \log_2(M_a)$. Here, $k_{f,p,a}$ can only take positive integer values and $M_{f,p,a}$ can only be equal to $2^{k_{f,p,a}}$. In the case where phase and amplitude are not used to encode data on, $M_p = M_a = 1$ and $k_p = k_a = 0$. This means the amplitude and phase are not changing.

Figure 4 shows the required signal-to-noise ratio to obtain a certain spectral efficiency at a symbol error rate of $P_{e_{PAFsk}} = 10^{-5}$, along with the theoretical spectral efficiency as defined by the Shannon capacity [45]. These values are obtained from Equations (6)-(10) using the relationship $SNR_s = kE_b/N_0$. Here, each curve for PAFsk-SIM is obtained with fixed M_a and M_p, whilst the modulation order in the frequency dimension is varied over $M_f = \{2, 4, 8, 16, 32, 64\}$. As expected, using additional signal dimensions (i.e., phase and amplitude for the medium and low priority data) does improve the spectral efficiency at the cost of higher signal power. It is worth highlighting that PAFsk-SIM is proposed for protecting high priority data against the debilitating OWC channel effects and this comes at the expense of spectral efficiency as Fig. 4 illustrates. Using FSK-SIM as a baseline, PAFsk-SIM can achieve
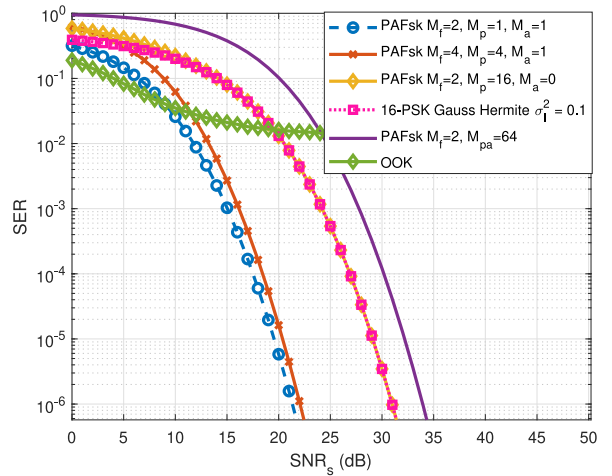
higher energy efficiency and higher spectral efficiency in comparison. To achieve an SER of 10^{-5}, PAFsk-SIM with $M_f = 4, M_p = 4, M_a = 1$ requires an E_b/N_0 of 7.65 dB while 16-FSK-SIM requires 0.61 dB more E_b/N_0 to attain the same SER. The most spectral efficient among the considered schemes is M_p-PSK -SIM, however, it also requires the highest energy per bit. For example, from Figures 4 and 5, a 16-PSK-SIM (i.e., $M_f = M_a = 1$, $M_p = 16$) operating at a spectral efficiency of 4 bits/s/Hz requires an E_b/N_0 of 18.1 dB to achieve an SER of 10^{-5}. In comparison, the most spectral efficient PAFsk-SIM scheme operates at 3.5 bits/s/Hz but requires slightly lower E_b/N_0 of 17.9 dB.

V. PERFORMANCE IN FADING AND MULTIPATH CHANNELS
The error performance of PAFsk-SIM is evaluated in different channel conditions in this section.

A. PAFSK-SIM IN TURBULENCE INDUCED FADING CHANNEL
Thus far, the symbol error performances are only considered in an AWGN channel. These expressions can be extended to a fading channel by averaging the error performance over the turbulence induced intensity fluctuations. The general form for this process is:

$$P_{e_{PAFsk}ave} = \int_0^\infty P_{e_{PAFsk}}\left(\alpha^2 SNR\right)p_\alpha(\alpha)d\alpha, \tag{12}$$

where α is a random variable whose probability density function (PDF), $p_\alpha(\alpha)$ depicts the intensity fluctuations.

Here, the performance of PAFsk-SIM in turbulence induced fading channel is considered. This type of channel is typical of free-space optical communications, space laser systems and UOWC. In such systems, turbulence is often characterised by the log-normal distribution [46], [47], [48]

whose PDF is given by (13). This model is valid for weak turbulence with $\sigma_I^2 < 1.2$ [1].

$$p_\alpha(\alpha) = \frac{1}{\sqrt{2\pi\sigma_\alpha^2}\alpha}\exp\left(-\frac{\left(\ln(\alpha/\alpha_0) + \sigma_\alpha^2/2\right)^2}{2\sigma_\alpha^2}\right), \quad (13)$$

where σ_α^2 is the log-irradiance variance, and $\mu = -\frac{\sigma_\alpha^2}{2}$. The log-irradiance variance is related to the scintillation index by $\sigma_\alpha^2 = \log(\sigma_I^2 + 1)$.

The analytical error performance of modulation schemes used in transmitting data over a channel with log-normal turbulence can be calculated using (12). Firstly the error performance of FSK-SIM is investigated as the base modulation technique of PAFsk-SIM. Thus, by combining (7) and (13), the average error probability, $P_{e_{\mathrm{f}}\mathrm{ave}}$ in log-normal fading channel is obtained as:

$$P_{e_{\mathrm{f}}\mathrm{ave}} = \int_0^\infty \sum_{n=1}^{M_f-1} (-1)^{n+1} C_n^{M_f-1} \frac{1}{n+1}\exp\left(-\frac{n\mathrm{SNR}_s}{(n+1)}\right)$$
$$\times \frac{1}{\sqrt{2\pi\sigma_\alpha^2}\alpha}\exp\left(-\frac{\left(\ln(\alpha/\alpha_0) + \sigma_\alpha^2/2\right)^2}{2\sigma_\alpha^2}\right)\mathrm{d}\alpha. \quad (14)$$

While this expression does not have a closed form solution, an accurate approximation can be obtained via Gauss-Hermite quadrature [49]:

$$\int_0^\infty f(x)\exp\left(-bx^2\right)\mathrm{d}x = \sum_{i=1}^\kappa \upsilon_i f(z_i), \quad (15)$$

where z_i and υ_i are the zeros of the κth order Hermite polynomial and corresponding weights respectively. Following variable change and simplification of the constant terms, $P_{e_{\mathrm{f}}\mathrm{ave}}$ becomes:

$$P_{e_{\mathrm{f}}\mathrm{ave}} = \sum_{i=1}^\kappa \left[\upsilon_i \sum_{n=1}^{M_f-1} (-1)^{n+1} C_n^{M_f-1} \frac{1}{n+1}\right.$$
$$\left.\times \exp\left(-\frac{n\gamma\alpha_i^2}{(n+1)}\right)\right], \quad (16)$$

where $\gamma = I_0^2\mathrm{SNR}_s/2$, $I_0 = \exp(-\sigma_I^2/2)$ and $\alpha_i = \exp(\sqrt{2}z_i\sigma_\alpha - \sigma_\alpha^2/2)$.

For the case of high and medium priority transmission only, (i.e., both the frequency and the phase of $x(t)$ modulated but not its amplitude), the error probability is:

$$P_{e_{\mathrm{PAFsk}}\mathrm{ave}} = \int_0^\infty \left(P_{e_{\mathrm{f}}} + P_{e_{\mathrm{p}}} - P_{e_{\mathrm{f}}}P_{e_{\mathrm{p}}}\right)$$
$$\times \frac{1}{\sqrt{2\pi\sigma_\alpha^2}\alpha}\exp\left(-\frac{\left(\ln(\alpha_i/\alpha_0) + \sigma_\alpha^2/2\right)^2}{2\sigma_\alpha^2}\right)\mathrm{d}\alpha, \quad (17)$$

Here, the term $P_{e_{\mathrm{f}}}P_{e_{\mathrm{p}}} \longrightarrow 0$ as SNR_s increases and therefore it is omitted. The resulting expression is solved via Gauss-Hermite approximation:

$$P_{e_{\mathrm{PAFsk}}} = \frac{1}{\sqrt{\pi}}\sum_{i=1}^\kappa \left[\upsilon_i\left(\sum_{n=1}^{M_f-1} (-1)^{n+1} C_n^{M_f-1}\frac{1}{n+1}\right.\right.$$
$$\left.\left.\times \exp\left(-\frac{n\gamma\alpha_i^2}{(n+1)}\right) + \zeta Q\left(4\gamma\alpha_i^2\right)\sin\left(\frac{\pi}{M_p}\right)\right)\right], \quad (18)$$

where constant $\zeta = 1$ for $M_p \leq 4$ and $\zeta = 2$ for $M_p > 4$.

With all the three-dimensions of $x(t)$ modulated, the average symbols error in a log-normal fading channel becomes as shown in (19), shown at the bottom of the page.

Figure 5 presents the SER performances of PAFsk-SIM with $M_f = 2$, $M_p = 1$, $M_a = 1$; $M_f = 4$, $M_p = 4$, $M_a = 1$; $M_f = 2$, $M_p = 16$, $M_a = 1$; $M_f = 1$, $M_p = 16$, $M_a = 1$ and $M_f = 2$, $M_{pa} = 64$ obtained from (19) in comparison with OOK. The data modulated on the frequency and phase are shown to be resilient against the effects of turbulence induced fading when compared to the baseline OOK. Thus the PAFsk-SIM levels can be increased to increase the throughput of the system. Amplitude can also be used for this purpose as long as channel estimations can be carried out. Comparatively, OOK with fixed threshold detection is unable to establish a reliable communications link as the its severely affected by turbulence and its SER performance converges to a value above 10^{-2}. When the data is modulated on the phase along with frequency (PAFsk-SIM with $M_f = 2$, $M_p = 16$, $M_a = 1$), the SER curve overlaps with that of when the information is solely encoded on the phase (PAFsk-SIM $M_f = 1$, $M_p = 16$, $M_a = 1$ (16-PSK-SIM)) when SNR is greater than 15 dB. This shows that, in comparison to modulating the phase of the subcarrier alone, there is no SNR penalty for modulating the phase along with the frequency and provides a higher energy efficiency. With respect to performance in noise limited channel shown in Fig. 3, the PAFsk-SIM with $M_f = 4$, $M_p = 4$, $M_a = 1$ incurred SNR

$$P_{e_{\mathrm{PAFsk}}\mathrm{ave}} = \frac{1}{\sqrt{\pi}}\sum_{i=1}^\kappa \left[\upsilon_i\left(\sum_{n=1}^{M_f-1} (-1)^{n+1} C_n^{M_f-1}\frac{1}{n+1}\exp\left(\frac{n\gamma\alpha_i^2}{(n+1)}\right)\right)\right.$$
$$\left.+ \left(1 - \left(1 - 2\left(1 - \frac{1}{\sqrt{M_{\mathrm{pa}}}}\right)Q\left(\sqrt{\frac{3}{M_{\mathrm{pa}}-1}\alpha_i^2\mathrm{SNR}_s}\right)\right)^2\right)\right] \quad (19)$$
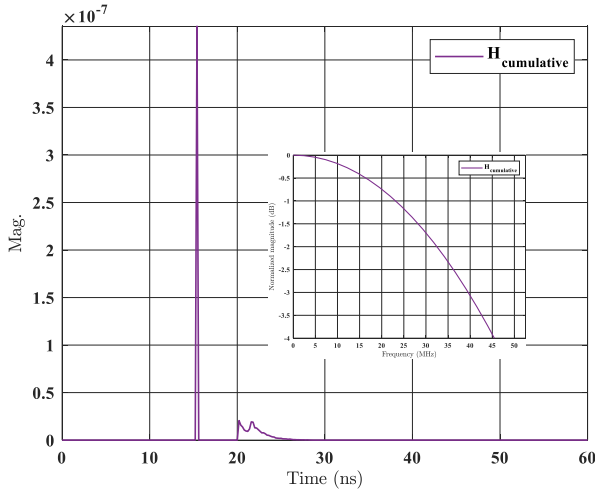
FIGURE 6. Frequency response with impulse response inset of the second degree multipath channel.

FIGURE 7. Error performance of PAFsk-SIM in second order multipath channel with OOK as benchmark.

penalty of 7.14 dB at an SER value of 10^{-6} due to turbulence induced fading with $\sigma_I^2 = 0.1$.

B. INDOOR MULTIPATH CHANNEL

In this section, an indoor VLC channel with second degree multipath propagation is considered. The degree of multipath refers to the number of possible indirect paths the signal can take before arriving at the receiver. To illustrate, a system with a single LED and a photodiode (PD) positioned at coordinates (3.75, 3.75, 3) and (1, 1, 0.5) respectively in a room with dimensions (5, 5, 3) m is considered. The walls; floor; and ceiling have respective reflectivities of $\rho_{wall} = 0.83$; $\rho_{floor} = 0.48$; $\rho_{ceiling} = 0.63$ as in [38]. The channel impulse response (CIR), along with corresponding frequency response, is given in Fig. 6. The CIR consisting of line of sight (LOS) and non-line-of-sight (NLOS) components is convolved with the desired transmission signal and noise is added in order to model data transmission through the channel.

The BER performance of PAFsk-SIM, along with OOK, are shown in Fig. 7 for the second order multipath channel. The CIR is sampled at 5 Gsam/s and for illustration only, the data rate is 62.5 and 125 Mbps for OOK; and 250, 500, 500, 750 Mbps for PAFsk-SIM with $\{M_f = 4, M_p = M_a = 1$ (4-FSK-SIM)\}, $\{M_f = 1, M_p = 4, M_a = 1$ (4-PSK-SIM)\}, $\{M_f = M_p = 4, M_a = 1\}$ and $\{M_f = M_{pa} = 16\}$ respectively. From the figure, it can be seen that OOK suffers a huge performance degradation with an SER $> 10^{-1}$ at the transmission rate of 125 Mbps and thus, a reliable communication link cannot be established. One solution is to increase the OOK symbol duration which reduces the transmission rate. It is shown that at the transmission rate of 62.5 Mbps, an SER of 10^{-6} can be achieved at an SNR$_s$ of 29 dB. In contrast, PAFsk-SIM is able to offer some resilience against ISI. The high and medium priority data encoded on the frequency (e.g., as in $M_f = 4, M_p = M_a = 1$) and phase (e.g., as in $M_f = M_p = 4, M_a = 1$) are able to
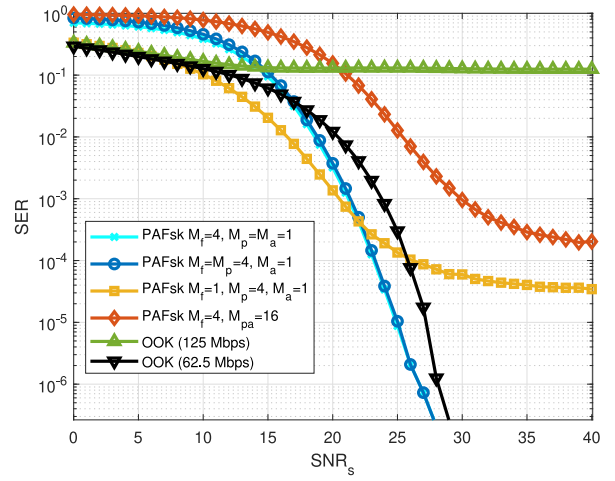
achieve an SER of 10^{-6} with 26.3 dB and 26.5 dB. For the latter case, the power penalty due to multipath effect in comparison with the AWGN scenario in Fig. 3 is 6.6 dB. Lower priority data modulated on the amplitude is affected severely from the multipath effect leading to the SER to converge to about 10^{-4}. Meanwhile, when only the phase is used to encode data, as in $M_f = 1, M_p = 4, M_a = 1$ (4-PSK-SIM), the SER converges to a value above 10^{-5}. While this value is below the FEC limit, the convergence to an error floor highlights the destructive effect of the multipath effect on the signal. Comparatively, PAFsk-SIM with $M_f = 4, M_p = 4, M_a = 1$ can achieve anSER of 10^{-6} at an SNR$_s$ value of 26.7 dB. This can be attributed to the resilience of the baseline FSK scheme.

Effects of the multipath propagation can be reduced with the use of cyclic prefix (CP) at the cost of additional overhead. Figure 8 shows the performance of SIM based schemes with CP of 30% signal length in the second order multipath channel. PAFsk-SIM with $M_f = 1, M_p = 4, M_a = 1$ (4-PSK-SIM) and $M_f = 1, M_{pa} = 16$ benefit the most from the application of CP as they are severely affected by the multipath effect and achieve an SER of 10^{-6} at an SNR$_s$ of 24.85 dB and 32.96 dB respectively. PAFsk-SIM with $M_f = 4, M_p = M_a = 1$ and $M_f = M_p = 4, M_a = 1$, with the addition of CP, are able to achieve an SER of 10^{-6} at an SNR$_s$ of 25.92 dB which is 0.78 dB less than without CP. Therefore, in scenarios where CP overhead can be afforded in a system, PAFsk-SIM with $M_f = 1, M_p = 4, M_a = 1$ (4-PSK-SIM) is optimal among the schemes considered. Meanwhile, PAFsk-SIM with $M_f = M_p = 4, M_a = 1$ is optimal for systems where additional overhead cannot be afforded.

C. MULTIPLE SCATTERING CHANNEL

This section considers a channel where the transmitted photons experience multiple scattering events, such as in UOWC or an FSO link in foggy conditions. Signals travelling
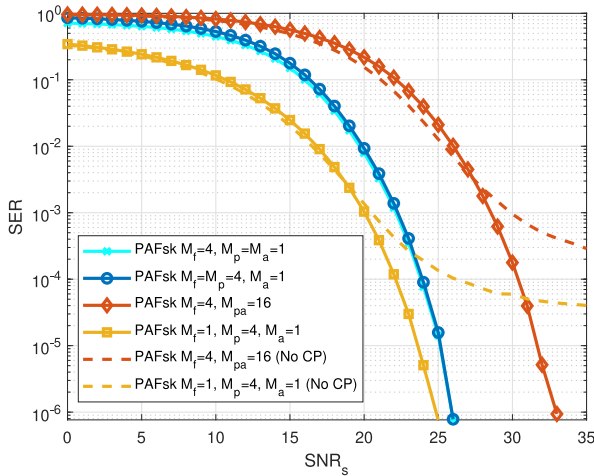
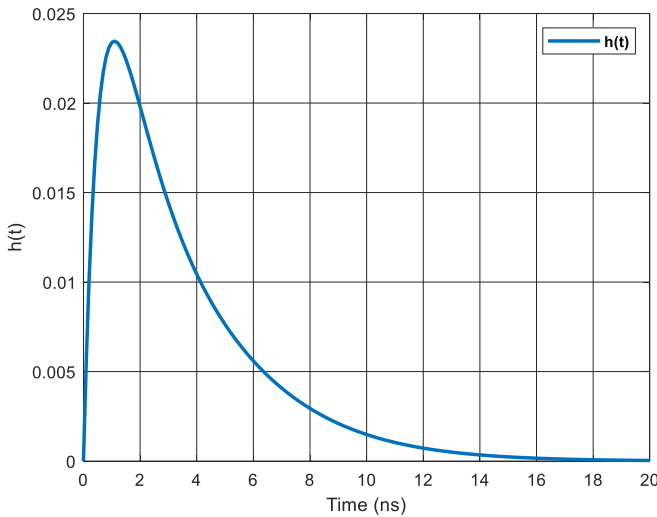**FIGURE 8.** Error performance of PAFsk-SIM with CP in second order multipath channel.

FIGURE 9. CIR of a 15m turbid harbour water link.

FIGURE 10. SNR per bit required to achieve different data rates at BER= 10^{-6} in multiple scattering channel.

in a channel with multiple scattering experience a time dispersion and consequently bandwidth limitation. The CIR of a multiple scattering UOWC channel can be described by the double-Gamma function (DGF) [43], [50]:

$$h(t) = C_1 t \exp(-C_2 t) + C_3 t \exp(-C_4 t), \qquad (20)$$

where $C_i, i = 1, 2, 3, 4$ are fitting coefficients related to the channel conditions. For illustration purposes, this study considers a DGF with $C_{1,2,3,4} = \{8.9, 1.2 \times 10^9, 2.4, 4.5 \times 10^6\}$ that represents turbid harbour water as in [51]. The resulting CIR is shown in Fig. 9. For this channel, photons arriving at different times due to scattering result in an root mean squared (RMS) delay spread, $\tau_{\text{RMS}} = 1.6$ ns.

The performance of PAFsk-SIM, in comparison with OOK, is evaluated in this channel via MC simulations. Transmission are carried out at different data rates and energy per bit values required for the transmission to achieve a BER of 10^{-6} are shown in Fig. 10. It is observed that, OOK is significantly affected by the temporal dispersion caused
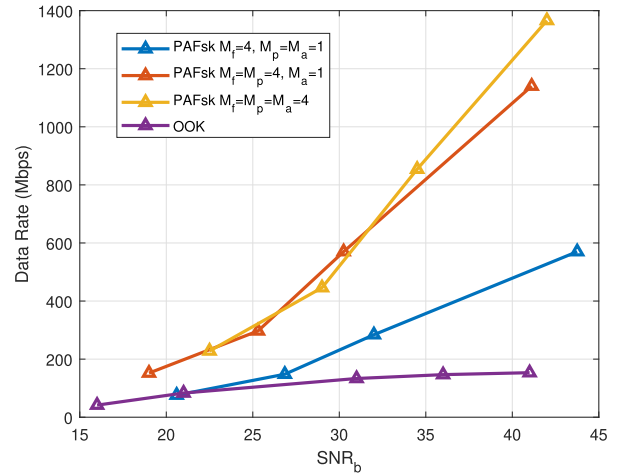
by the channel. Using OOK, maximum data rate of 153 Mbps is achieved at $E_b/N_0 = 41$ dB. Increasing the signal power beyond this has not yielded any improvement in the system performance as ISI is the dominant effect in this region of operation. For PAFsk-SIM, CP can be added to offer resilience against the channel dispersion. In this work, a CP with length equal to 30% of the signal length is used.

A comparison of highest data rates achieved at a BER value of 10^{-6} and the E_b/N_0 required for this transmission is presented in Fig. 10. Frequency only modulated scheme, $M_f = 4, M_p = M_a = 1$ starts with a comparable data rate and E_b/N_0 requirement as OOK, however as the E_b/N_0 increases so does the data rate of PAFsk-SIM. As OOK is more severely affected by the channel effect, increasing the transmission power does not benefit the system performance. Medium and low priority data can be further modulated and the resultant hierarchical modulation achieves 1.14 and 1.36 Gbps data rate with SNR per bit values of 41.12 dB and 42 dB respectively.

VI. EXPERIMENTAL CASE STUDY - UNDERWATER CHANNEL

This section discusses the experimental implementation of the PAFsk-SIM schemes, using the UOWC turbulence induced fading channel as a case study.

A block diagram of the system setup is presented in Fig. 11, along with the system frequency response. The experimental testbed is shown in Fig. 12 and the experimental parameters are presented in Table 1. The transmitter side consists of a Keysight m8195a arbitrary waveform generator (AWG), an Osram PL450b laser diode (LD), DC power supply, a bias-T, and a collimation lens. Here, random data bits are generated and used to implement hierarchical modulation offline using MATLAB software. The resulting signal is then sent to the AWG where it is sampled prior transmission. This modulated electrical signal with peak-to-peak voltage of 0.5 V is combined with 30 mA DC

TABLE 1. Experimental parameters.

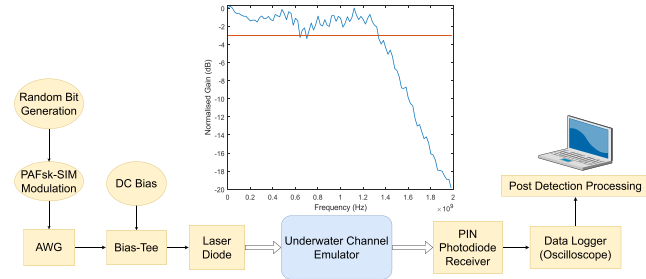| Parameter	Value
Tank Dimensions	$1.5 \times 0.5 \times 0.5$ m^3
LD Centre Wavelength (λ)	450 nm
LD Bias Current	30 mA
Signal V$_{pp}$	0.5 V
AWG Sampling Rate	64 Gsam/s
Oscilloscope Sampling Rate	40 Gsam/s

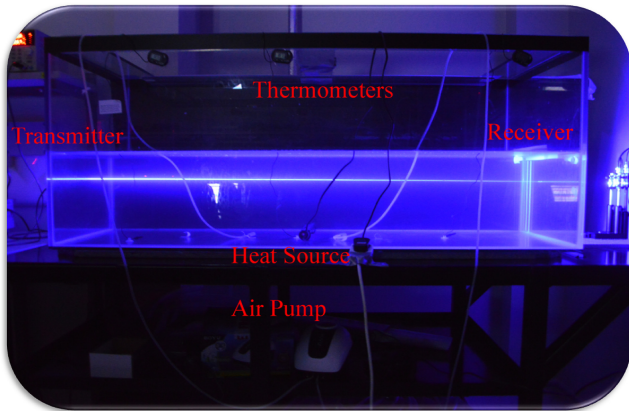**FIGURE 11.** Experimentation process with frequency response of the system in-layed.

FIGURE 12. Experimental testbed.

current using a bias-tee to drive the laser diode. The emitted optical beam is finally collimated for propagation through the underwater channel emulator (UCE). The UCE consists of a $1.5 \times 0.5 \times 0.5$ m^3 water tank in which a heat source may be placed along the link. This heater introduces a temperature inhomogeneity to the medium which induces underwater turbulence within the UCE, as in our previous work in [52]. At the receiver side, the optical beam is received by a Femto HSPR-X-I-1G4-SI PIN photoreceiver, followed by an Agilent DSA90804A oscilloscope. The received electrical signal is then is analysed in MATLAB offline.

Due to the long coherence time of underwater turbulence, this data transmission is repeated for 1000 iterations in order to gather a true representation of the random channel. The measured performance of the PAFsk-SIM UOWC system over a range of turbulence conditions is presented in Fig. 13. This figure clearly shows that high priority data encoded on the subcarrier frequency are shielded from the turbulence
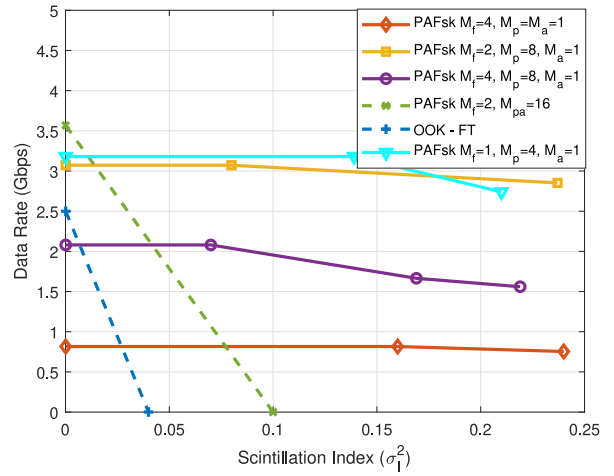

FIGURE 13. Highest achievable data rate within FEC limit for different PAFsk-SIM modulation order in comparison with OOK baseline.

induced fading in the channel. The data rate of 0.75 Gbps is maintained across different levels of turbulence of up to $\sigma_I^2 = 0.25$. Expectedly, the low priority data on the subcarrier signal amplitude suffer performance degradation in the presence of channel fading. An indication of this is the $M_f = 2, M_p = 4, M_a = 4$ whose aggregate data rate is 3.5 Gbps in no fading noise limited condition ($\sigma_I^2 = 0$) but cannot establish a communication link with a BER within the FEC limit in fading channel with $\sigma_I^2 > 0.1$. Using the subcarrier phase for medium priority provided some level of resilience while enhancing the spectral efficiency over using only the subcarrier signal frequency for data transmission. For example, PAFsk-SIM with $M_f = 2, M_p = 8, M_a = 1$, an aggregate transmission speed of 3.1 Gbps is recorded in noise limited conditions and this only reduced to 2.85 Gbps in turbulence induced fading with $\sigma_I^2 = 0.24$. This resilience is also observed in PAFsk-SIM with $M_f = 1, M_p = 4, M_a = 1$ (4-PSK-SIM) as the maximum achieved data rate can be reliably preserved in the presence of turbulence with a drop from 3.1 Gbps at $\sigma_I^2 = 0$ to 2.74 Gbps at $\sigma_I^2 = 0.21$. In contrast, transmission using OOK with fixed threshold (FT) decoding is shown to be very unreliable in the presence of turbulence as the communication link breaks down for a $\sigma_I^2 > 0.04$. The phase and frequency modulated systems prove resilient against turbulence induced fading as the decision boundary between the information symbols are not affected. Information can be encoded on the subcarrier signal frequency in systems where channel estimation is not possible and higher data rates can be achieved by encoding the information on the subcarrier signal phase.

VII. CONCLUSION
This paper presented the performance analysis of the PAFsk-SIM technique in hostile environments. This technique is evaluated analytically, through simulation and in experimental studies. Through this analysis, FSK-SIM which is the base modulation scheme of PAFsk-SIM, is shown to be the

most energy efficient and highly resilient against malicious channel effects. However, it has a low spectral efficiency. This can be improved upon through the development of PAFsk-SIM as an extension of FSK-SIM. PAFsk-SIM is demonstrated for the first time, and is shown to be resilient against turbulence induced fading. Simulation results in an indoor multipath channel further show the potential of PAFsk-SIM as a modulation technique that is resilient to the hostile ISI channel effect. PAFsk-SIM has shown its ability to preserve the energy efficiency of FSK-SIM while boosting its transmission rate capabilities, maintaining the power requirements while increasing the number of bits encoded. Utilising phase and amplitude to increase the spectral efficiency of the system is shown to be optimal in achieving highest data rates in applications where channel estimation can be carried out reliably. These results provide insight on OWC system design in practical scenarios with realistic channel effects.

ACKNOWLEDGMENT

REFERENCES

[1] Z. Ghassemlooy, W. Popoola, and S. Rajbhandari, *Optical Wireless Communications: System and Channel Modelling With MATLAB*, 1st ed. Boca Raton, FL, USA: CRC Press, Inc., 2012.

[2] D. Tsonev, S. Videv, and H. Haas, "Light fidelity (Li-Fi): Towards all-optical networking," in *Broadband Access Communication Technologies VIII*, B. B. Dingel and K. Tsukamoto, Eds., vol. 9007. Bellingham, WA, USA: SPIE, 2014, Art. no. 900702. [Online]. Available: https://doi.org/10.1117/12.2044649

[3] H. Kaushal and G. Kaddoum, "Underwater optical wireless communication," *IEEE Access*, vol. 4, pp. 1518–1547, 2016.

[4] H. Abuella et al., "Hybrid RF/VLC systems: A comprehensive survey on network topologies, performance analyses, applications, and future directions," *IEEE Access*, vol. 9, pp. 160402–160436, 2021.

[5] A. Trichili et al., "Retrofitting FSO systems in existing RF infrastructure: A non-zero-sum game technology." 2021. [Online]. Available: http://hdl.handle.net/10754/669218

[6] F. V. Corral, C. Cuenca, and I. Soto, "Design of an optical wireless network using free space optics technology (FSO), in 5G/6G networks environment," in *Proc. IEEE Int. Conf. Autom./XXIV Congr. Chilean Assoc. Automat. Control (ICA-ACCA)*, 2021, pp. 1–5.

[7] H. Haas et al., "Introduction to indoor networking concepts and challenges in LiFi," *J. Opt. Commun. Netw.*, vol. 12, no. 2, pp. A190–A203, Feb. 2020.

[8] H.-H. Lu et al., "A two-way 224-Gbit/s PAM4-based fibre-FSO converged system," *Sci. Rep.*, vol. 12, no. 1, p. 360, 2022.

[9] W.-S. Tsai, H.-H. Lu, H.-W. Wu, C.-W. Su, and Y.-C. Huang, "A 30 gb/s PAM4 underwater wireless laser transmission system with optical beam reducer/expander," *Sci. Rep.*, vol. 9, no. 1, p. 8605, 2019.

[10] Y. Zhou et al., "Common-anode LED on a Si substrate for beyond 15 Gbit/s underwater visible light communication," *Photon. Res.*, vol. 7, no. 9, pp. 1019–1029, Sep. 2019. [Online]. Available: http://opg.optica.org/prj/abstract.cfm?URI=prj-7-9-1019

[11] W. O. Popoola and Z. Ghassemlooy, "BPSK subcarrier intensity modulated free-space optical communications in atmospheric turbulence," *J. Lightw. Technol.*, vol. 27, no. 8, pp. 967–973, Apr. 2009.

[12] P. Hahn, "Theoretical diversity improvement in multiple frequency shift keying," *IRE Trans. Commun. Syst.*, vol. 10, no. 2, pp. 177–184, Jun. 1962.

[13] J. Armstrong, "OFDM for optical communications," *J. Lightw. Technol.*, vol. 27, no. 3, pp. 189–204, Feb. 2009. [Online]. Available: http://opg.optica.org/jlt/abstract.cfm?URI=jlt-27-3-189

[14] S. Habibi, M. Omidi, F. S. Tabataba, and E. Yazdian, "An overview: Orthogonal frequency division multiplexing techniques for visible light communication systems," in *Proc. 4th West Asian Symp. Opt. Millimeter-Wave Wireless Commun. (WASOWC)*, 2022, pp. 01–06.

[15] X. Song, J. Cheng, and M.-S. Alouini, "BER of subcarrier MPSK/MDPSK modulated OWC systems in gamma-gamma turbulence," in *Proc. IEEE Globecom Workshops (GC Wkshps)*, 2013, pp. 1041–1045.

[16] M. Wetz, I. Periša, W. G. Teich, and J. Lindner, "Robust transmission over fast fading channels on the basis of OFDM-MFSK," *Wireless Pers. Commun.*, vol. 47, no. 1, pp. 113–123, 2007.

[17] M. J. Khan, A. W. Azim, Y. Le Guennec, G. Maury, and L. Ros, "Theoretical and experimental analysis of asymmetrically clipped-FSK VLC system," *IEEE Photon. J.*, vol. 14, no. 3, Jun. 2022, Art. no. 7326409.

[18] E. Guler, C. Geldard, A. Baldwin, and W. Popoola, "A demonstration of frequency-shift keying in underwater wireless optical communications," in *Proc. Conf. Lasers Electro-Opt.*, 2022, Art. no. JW3B.104. [Online]. Available: http://opg.optica.org/abstract.cfm?URI=CLEO_SI-2022-JW3B.104

[19] X. Zhang, Z. Babar, P. Petropoulos, H. Haas, and L. Hanzo, "The evolution of optical OFDM," *IEEE Commun. Surveys Tuts.*, vol. 23, no. 3, pp. 1430–1457, 3rd Quart., 2021.

[20] X. Liu, J. Zhou, N. Huang, and W. Zhang, "Improved receivers for optical wireless OFDM: An information theoretic perspective," *IEEE Trans. Commun.*, vol. 70, no. 7, pp. 4439–4453, Jul. 2022.

[21] T. Z. Gutema, H. Haas, and W. O. Popoola, "WDM based 10.8 Gbps visible light communication with probabilistic shaping," *J. Lightw. Technol.*, vol. 40, no. 15, pp. 5062–5069, Aug. 2022.

[22] J. Du et al., "A comprehensive performance comparison of DFT-S DMT and QAM-DMT in UOWC system in different water environments," *IEEE Photon. J.*, vol. 13, no. 1, Feb. 2021, Art. no. 7900211.

[23] Z. Wang, L. Zhang, Z. Wei, Y. Dong, G. Wei, and H. Fu, "Beyond 25 Gbps OFDM UOWC system based on green and blue laser diodes with wavelength and polarization multiplexing," in *Proc. 9th Int. Conf. Commun. Broadband Netw.*, Feb. 2021, pp. 329–332.

[24] S. Huang et al., "Performance analysis of SPAD-based optical wireless communication with OFDM," *J. Opt. Commun. Netw.*, vol. 15, no. 3, pp. 174–186, 2023.

[25] R. Mesleh, H. Elgala, and H. Haas, "An overview of indoor OFDM/DMT optical wireless communication systems," in *Proc. 7th Int. Symp. Commun. Syst. Netw. Digit. Signal Process. (CSNDSP)*, 2010, pp. 566–570.

[26] M. Kong et al., "Real-time optical-wireless video surveillance system for high visual-fidelity underwater monitoring," *IEEE Photon. J.*, vol. 14, no. 2, Apr. 2022, Art. no. 7315609.

[27] M. Kong et al., "Toward automatic Subsea operations using real-time underwater optical wireless sensor networks," *IEEE Photon. J.*, vol. 14, no. 1, Feb. 2022, Art. no. 7308408.

[28] J. P. Loureiro, F. B. Teixeira, and R. Campos, "Adaptive and reliable underwater wireless video streaming using data muling," in *Proc. OCEANS San Diego–Porto*, 2021, pp. 1–10.

[29] J. I. de Oliveira Filho, A. Trichili, B. S. Ooi, M.-S. Alouini, and K. N. Salama, "Toward self-powered Internet of Underwater Things devices," *IEEE Commun. Mag.*, vol. 58, no. 1, pp. 68–73, Jan. 2020.

[30] M. Uysal, S. Ghasvarianjahromi, M. Karbalayghareh, P. D. Diamantoulakis, G. K. Karagiannidis, and S. M. Sait, "SLIPT for underwater visible light communications: Performance analysis and optimization," *IEEE Trans. Wireless Commun.*, vol. 20, no. 10, pp. 6715–6728, Oct. 2021.

[31] K. W. S. Palitharathna, H. A. Suraweera, R. I. Godaliyadda, V. R. Herath, and Z. Ding, "Lightwave power transfer in full-duplex NOMA underwater optical wireless communication systems," *IEEE Commun. Lett.*, vol. 26, no. 3, pp. 622–626, Mar. 2022.

[32] S. Ammar, O. Amin, M.-S. Alouini, and B. Shihada, "Energy-aware underwater optical system with combined solar cell and SPAD receiver," *IEEE Commun. Lett.*, vol. 26, no. 1, pp. 59–63, Jan. 2022.

[33] R. Khalona, G. Atkin, and J. LoCicero, "On the performance of a hybrid frequency and phase shift keying modulation technique," *IEEE Trans. Commun.*, vol. 41, no. 5, pp. 655–659, May 1993.

[34] A. W. Azim, Y. Le Guennec, and L. Ros, "Hybrid frequency and phase-shift keying modulation for energy efficient optical wireless systems," *IEEE Wireless Commun. Lett.*, vol. 9, no. 4, pp. 429–432, Apr. 2020.

[35] C. T. Geldard, J. Thompson, and W. O. Popoola, "Empirical study of the underwater turbulence effect on non-coherent light," *IEEE Photon. Technol. Lett.*, vol. 32, no. 20, pp. 1307–1310, Oct. 2020.

[36] Z. Zeng, S. Fu, H. Zhang, Y. Dong, and J. Cheng, "A survey of underwater optical wireless communications," *IEEE Commun. Surveys Tuts.*, vol. 19, no. 1, pp. 204–238, 1st Quart., 2017.

[37] X. Sun et al., "A review on practical considerations and solutions in underwater wireless optical communication," *J. Lightw. Technol.*, vol. 38, no. 2, pp. 421–431, Jan. 2020.

[38] H. G. Olanrewaju, J. Thompson, and W. O. Popoola, "Performance of optical spatial modulation in indoor multipath channel," *IEEE Trans. Wireless Commun.*, vol. 17, no. 9, pp. 6042–6052, Sep. 2018.

[39] R. Qadar, W. B. Qaim, J. Nurmi, and B. Tan, "Effects of Multipath attenuation in the optical communication-based Internet of Underwater Things," *Sensors*, vol. 20, no. 21, p. 6201, Oct. 2020. [Online]. Available: https://www.ncbi.nlm.nih.gov/pmc/articles/PMC7663492/

[40] H. Mei, J. Ding, J. Zheng, X. Chen, and W. Liu, "Overview of vehicle optical wireless communications," *IEEE Access*, vol. 8, pp. 173461–173480, 2020.

[41] C. D. Mobley. "Oceans optics Web book." 2020. [Online]. Available: https://www.oceanopticsbook.info/

[42] Z. Ghassemlooy, S. Arnon, M. Uysal, Z. Xu, and J. Cheng, "Emerging optical wireless communications-advances and challenges," *IEEE J. Sel. Areas Commun.*, vol. 33, no. 9, pp. 1738–1749, Sep. 2015.

[43] C. T. Geldard, J. Thompson, E. Leitgeb, and W. O. Popoola, "Optical wireless underwater channel modelling in the presence of turbulence," in *Proc. IEEE Brit. Irish Conf. Opt. Photon. (BICOP)*, 2018, pp. 1–4.

[44] J. Chen, C. T. Geldard, E. Guler, A. Hamilton, and W. O. Popoola, "An experimental demonstration of FSK-SIM-PDM underwater optical wireless communications," in *Proc. 6th Underwater Commun. Netw. Conf. (UComms)*, 2022, pp. 1–4.

[45] J. G. Proakis, *Digital Communications*. New York, NY, USA: Mcgraw-Hill, 2001.

[46] X. Zhu and J. Kahn, "Free-space optical communication through atmospheric turbulence channels," *IEEE Trans. Commun.*, vol. 50, no. 8, pp. 1293–1300, Aug. 2002.

[47] W. O. Popoola, Z. Ghassemlooy, J. I. H. Allen, E. Leitgeb, and S. Gao, "Free-space optical communication employing sub-carrier modulation and spatial diversity in atmospheric turbulence channel," *IET Optoelectron.*, vol. 2, pp. 16–23, Feb. 2008. [Online]. Available: https://digital-library.theiet.org/content/journals/10.1049/iet-opt_20070030

[48] E. Zedini, H. M. Oubei, A. Kammoun, M. Hamdi, B. S. Ooi, and M.-S. Alouini, "Unified statistical channel model for turbulence-induced fading in underwater wireless optical communication systems," *IEEE Trans. Commun.*, vol. 67, no. 4, pp. 2893–2907, Apr. 2019.

[49] M. Abramowitz and I. A. Stegun, *Handbook of Mathematical Functions With Formulas, Graphs, and Mathematical Tables*, U.S. Dept. Commer., Nat. Bureau Stand., Washington, DC, USA, 1972. [Online]. Available: https://personal.math.ubc.ca/~cbm/aands/abramowitz_and_stegun.pdf

[50] S. Tang, Y. Dong, and X. Zhang, "Impulse response modeling for underwater wireless optical communication links," *IEEE Trans. Commun.*, vol. 62, no. 1, pp. 226–234, Jan. 2014.

[51] C. T. Geldard, J. Thompson, and W. O. Popoola. "Effects of turbulence induced scattering on underwater optical wireless communications." 2020. [Online]. Available: https://arxiv.org/abs/2008.01152

[52] C. T. Geldard, E. Guler, A. Hamilton, and W. O. Popoola, "An empirical comparison of modulation schemes in turbulent underwater optical wireless communications," *J. Lightw. Technol.*, vol. 40, no. 7, pp. 2000–2007, Apr. 2022.